

An Orphan-cell-free Overset Method Based on Meshless MLS Approximation for Coupled Analysis of Overlapping Finite Element Substructures

Dong Ju Woo¹, Jin Oh Yang¹, Beom-Soo Kim¹, Seungsoo Lee¹ and Jin Yeon Cho²

Abstract: A new orphan-cell-free overset method is proposed to carry out the coupled analysis of overlapping finite element substructures. In the proposed overset method, the meshless MLS (Moving Least Squares) approximation is used to obtain the boundary data for the overlapped interface, whereas the Lagrange interpolation scheme has been commonly used in the conventional overset methods. The meshless character of MLS approximation makes it possible to overcome the problem of orphan-cell, which is often encountered in the conventional overset methods. Further, a new connectivity matrix solution procedure is developed to reduce the computational time in the coupled analysis as a part of the new overset method.

To justify the validity of the proposed method, the patch tests and the convergence tests are carried out for various overlapping models. The efficiency of the connectivity matrix solution procedure over the conventional iterative solving procedure is investigated, and the flexibility of the present overset method in dealing with the overlapping substructures is examined through the several overlapping models, including the case with the orphan-cell.

Keyword: Orphan-cell-free Overset Method, Coupled Analysis, Overlapping Substructures, Connectivity Matrix, Moving Least Squares Method.

1 Introduction

Nowadays, geometric shapes of structural systems have become more complicated due to the ever-increasing design requirements. As a result, the importance of geometric modeling has been emphasized more than ever for the efficient structural design and analysis, and considerable research efforts have been devoted to increase the modeling flexibility in the structural design and analysis.

These efforts include the automatic mesh-generation techniques [Li, Teng and Wan (2001); Chung, Choi and Kim (2003); Liu, Sun and Wang (2006)] and the coupled analysis methods [Aminpour, Ransom and McCleary (1995); Park and Fellippa (2000); Aminpour, Pageau and Shin (2001); Cho, et al. (2005); Vodička, Mantič and París (2007)]. Whereas the objectives of both methods are the same, the coupled structural analysis methods are based on a different concept from the automatic mesh-generation. While the automatic mesh-generation has focused on how to generate geometrically compatible finite element system, the coupled analysis method has focused on how to analyze the integrated system composed of geometrically incompatible finite element substructures.

Regarding the collaborative engineering, the concept inside the coupled analysis has a practical attractiveness. In real practice, the complex structural systems are usually modeled collaboratively in the form of substructures by several engineers, and there may be a geometric incompatibility between the substructures. Therefore, if it is possible to directly utilize the independently modeled finite element substructures for analyzing the integrated whole model with no regard to their

¹ Department of Aerospace Engineering, INHA University, Korea

² Corresponding Author, Associate Professor, Department of Aerospace Engineering, INHA University, 253 Yonghyun-Dong, Nam-Gu, Incheon, 402-751, Korea, E-mail: cji@inha.ac.kr

geometric incompatibilities, it could reduce the labor-intensive re-modeling procedure of the integrated system. This is the concept behind the coupled analysis method. Based on the idea, aforementioned various coupled analysis methods have been proposed to analyze the integrated system composed of independently modeled finite element substructures.

However, since these methods have been developed only to handle the nodal incompatibilities on the interfaces between the finite element substructures, these are not appropriate in dealing with the system composed of overlapping finite element substructures.

Traditionally overset method has been developed in the field of computational fluid dynamics to avoid the difficulties in generating a geometrically compatible grid system for a highly complex geometric domain as shown Fig.1 [Steger and Benek (1987); Cho, Kwon and Lee (1999); Lee, Park, Cho and Kwon (2000)]. In overset methods, after generating the grid system for each simple model, the set of whole grid systems is utilized to solve the complex problem for the complicated model with no regard to the overlapping between each grid system. Therefore, this concept is also very attractive in solid and structural engineering problems and it may be a good candidate to eliminate the tedious re-modeling procedure for the regions of overlapping. However, traditional overset method has a problem of interpolation arising from the existence of the so-called ‘orphan-cell’, because all of the previously developed overset methods rely on the mesh-dependent interpolation techniques such as the Lagrange interpolation scheme.

Due to the aforementioned reasons, a novel overset method, based on the meshless MLS (moving least squares) approximation [Lancaster and Salkauskas (1981); Atluri, Cho and Kim (1999); Nie, Atluri and Zuo (2006); Cho (2007)], is proposed in this paper, in order to eliminate the drawbacks of previous overset methods as well as to utilize the advantageous nature of overset method in handling the integrated system composed of overlapping finite element substructures.

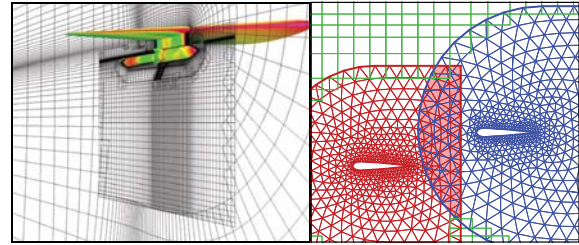


Figure 1: Examples of overset grid systems in the field of computational fluid dynamics.

2 Orphan-cell-free Overset Method

2.1 Schwarz Alternating Scheme

Originally, Schwarz alternating method was invented as an iterative method to solve the problem defined on the union of two overlapping sub-domains, and it evolved into the Schwarz-Neumann alternating method to obtain the solution for intersection of overlapping domains [Schwarz (1869); Lions (1987); Wang and Atluri (1996); Han and Atluri (2002); Wijesinghe and Hadjiconstantinou (2004)]. Most of overset methods are basically based on the Schwarz alternating method to handle the union of overlapping sub-domains.

For a linear elliptic problem, the Schwarz alternating procedure for union of overlapping sub-domains can be described as follows.

Let us consider the linear elliptic equation in the domain Ω .

$$Lu = f \quad \text{in } \Omega \quad (1)$$

$$\begin{aligned} u &= \bar{u} \quad \text{on } \partial\Omega_e \quad \text{and} \\ \delta_n u &= \bar{s} \quad \text{on } \partial\Omega_n \end{aligned} \quad (2)$$

where L is the linear elliptic operator and δ_n is the Neumann operator for the natural boundary condition. u is unknown, and f is a given function. $\partial\Omega_e$ and $\partial\Omega_n$ are the essential and natural boundaries of domain Ω , respectively, and \bar{u} and \bar{s} are the prescribed values along the essential and natural boundaries.

Further, the domain Ω is supposed to be composed of overlapping sub-domains Ω_1 and Ω_2 (i.e., $\Omega = \Omega_1 \cup \Omega_2$), as shown in Fig. 2. In Fig.

2, $\partial\Omega_\alpha$ denotes the boundary of each sub-domain Ω_α , and Γ_α ($1 \leq \alpha \leq 2$) is the overlapped interface, which is the part of boundary of each sub-domain Ω_α , contained in the interior of the entire domain Ω .

Then the Schwarz alternating procedure for this problem can be summarized as follows.

[Initialization step]

Set the value of $u_2^{(0)}$ on Γ_1 as zero.

[Iteration step]

Do $k=0$

- i) For the sub-domain Ω_1 , obtain $u_1^{(k+1)}$ by solving Eq. (3) with the boundary conditions (4).

$$Lu_1^{(k+1)} = f \text{ in } \Omega_1 \quad (3)$$

$$\begin{cases} u_1^{(k+1)} = u_2^{(k)} & \text{on } \Gamma_1 \\ u_1^{(k+1)} = \bar{u} & \text{on } \partial\Omega_1^e = \partial\Omega_e \cap \partial\Omega_1 \\ \delta_n u_1^{(k+1)} = \bar{s} & \text{on } \partial\Omega_1^n = \partial\Omega_n \cap \partial\Omega_1 \end{cases} \quad (4)$$

- ii) For the sub-domain Ω_2 , obtain $u_2^{(k+1)}$ by solving Eq. (5) with the boundary conditions (6).

$$Lu_2^{(k+1)} = f \text{ in } \Omega_2 \quad (5)$$

$$\begin{cases} u_2^{(k+1)} = u_1^{(k+1)} & \text{on } \Gamma_2 \\ u_2^{(k+1)} = \bar{u} & \text{on } \partial\Omega_2^e = \partial\Omega_e \cap \partial\Omega_2 \\ \delta_n u_2^{(k+1)} = \bar{s} & \text{on } \partial\Omega_2^n = \partial\Omega_n \cap \partial\Omega_2 \end{cases} \quad (6)$$

- iii) Construct the solution over the entire domain by combining the solutions $u_1^{(k+1)}$ and $u_2^{(k+1)}$ of each sub-domain.

$$\mathbf{u}^{(k+1)} = \begin{cases} u_1^{(k+1)} \\ u_2^{(k+1)} \end{cases} \quad (7)$$

- iv) If the relative error norm (8) is smaller than the tolerance ε_{tol} , then terminate the iteration.

$$e^{(k+1)} = \frac{\|\mathbf{u}^{(k+1)} - \mathbf{u}^{(k)}\|}{\|\mathbf{u}^{(k+1)}\|} \leq \varepsilon_{tol} \quad (8)$$

If not, set $k = k + 1$

Continue

The Schwarz alternating procedure can be also rewritten in discretized form, after its finite element approximation. For this purpose, consider a finite element system composed of two overlapping substructures as shown in Fig. 3, and suppose that the nodal variables for each sub-domain are decomposed into \mathbf{U}_α , $\mathbf{U}_{\Gamma_\alpha}$, and $\mathbf{U}_{\partial\Omega_\alpha^e}$ ($1 \leq \alpha \leq 2$) as shown in Fig. 4. Then, the Schwarz alternating procedure for this overlapping finite element model can be written as follows.

[Initialization step]

Assign the essential boundary conditions to each sub-domain by using the essential boundary condition given for the global domain.

$$\begin{cases} \mathbf{U}_{\partial\Omega_1^e} = \bar{\mathbf{U}}_{\partial\Omega_1^e} & \text{for } \partial\Omega_e \cap \partial\Omega_1 \\ \mathbf{U}_{\partial\Omega_2^e} = \bar{\mathbf{U}}_{\partial\Omega_2^e} & \text{for } \partial\Omega_e \cap \partial\Omega_2 \end{cases} \quad (9)$$

Set the value of $\mathbf{U}_{\Gamma_1}^{(1)}$ on Γ_1 as zero.

[Iteration step]

Do $k=0$

- i) For the sub-domain Ω_1 , obtain $\mathbf{U}_1^{(k+1)}$ such that

$$[\mathbf{K}_{11} \quad \mathbf{K}_{1\Gamma_1}] \begin{Bmatrix} \mathbf{U}_1 \\ \mathbf{U}_{\Gamma_1} \end{Bmatrix}^{(k+1)} = \mathbf{F}_1 \quad (10)$$

$$\mathbf{U}_{\Gamma_1}^{(k+1)} = \Lambda \left(\mathbf{U}_2^{(k)}, \mathbf{U}_{\Gamma_2}^{(k)}, \bar{\mathbf{U}}_{\partial\Omega_2^e} \right) \text{ for } k \geq 1 \quad (11)$$

- ii) For the sub-domain Ω_2 , obtain $\mathbf{U}_2^{(k+1)}$ such that

$$[\mathbf{K}_{22} \quad \mathbf{K}_{2\Gamma_2}] \begin{Bmatrix} \mathbf{U}_2 \\ \mathbf{U}_{\Gamma_2} \end{Bmatrix}^{(k+1)} = \mathbf{F}_2 \quad (12)$$

$$\mathbf{U}_{\Gamma_2}^{(k+1)} = \Lambda \left(\mathbf{U}_1^{(k+1)}, \mathbf{U}_{\Gamma_1}^{(k+1)}, \bar{\mathbf{U}}_{\partial\Omega_1^e} \right) \quad (13)$$

- iii) Construct the solution over the entire domain.

$$\mathbf{U}^{(k+1)} = \begin{Bmatrix} \mathbf{U}_1 \\ \mathbf{U}_{\Gamma_1} \\ \mathbf{U}_2 \\ \mathbf{U}_{\Gamma_2} \end{Bmatrix}^{(k+1)} \quad (14)$$

- iv) If the relative error norm is smaller than the tolerance ϵ_{tol} , then terminate the iteration.

$$e^{(k+1)} = \frac{\|\mathbf{U}^{(k+1)} - \mathbf{U}^{(k)}\|}{\|\mathbf{U}^{(k+1)}\|} \leq \epsilon_{tol} \quad (15)$$

If not, set $k = k + 1$

Continue

where $\Lambda(\cdot)$ represents an interpolation procedure, and the superscript denotes the iteration number. In the above, the essential and natural boundary conditions of Eq. (2) are already taken into account in constructing the stiffness matrices and load vectors of each sub-domain.

It is noted that the result of the previous step obtained in the neighboring sub-domain is utilized to interpolate the essential boundary values on the overlapped interface $\Gamma_\alpha (1 \leq \alpha \leq 2)$ for the next step. In numerical calculation, it occurs frequently that the nodal points on the overlapped interface Γ_α of the sub-domain Ω_α may not coincide with the nodal points of the other sub-domain, as shown in Fig. 3. Thus, it becomes difficult to directly use the results of the previous step as the essential boundary value on Γ_α for the next step, and it becomes inevitable to utilize an interpolation scheme $\Lambda(\cdot)$. Customarily, the Lagrange interpolation scheme has been widely utilized in the context of the overset method. However, the Lagrange interpolation scheme has a problem because of its mesh-dependent character. For example, let us assume that there is a boundary cell (so-called ‘orphan-cell’) in the sub-domain A, which is not contained in the other sub-domain B as shown in Fig. 5. Then, it is impossible to interpolate the value at the nodal point of interest C by using the solution of the sub-domain B through the Lagrange interpolation scheme. To overcome this drawback, this work employs the MLS (moving least squares) approximation instead of the Lagrange interpolation scheme. It is noted that the meshless feature of MLS scheme makes it possible to interpolate the value at the point of interest with no regard to the existence of orphan-cell. In the next section, the MLS method is briefly reviewed.

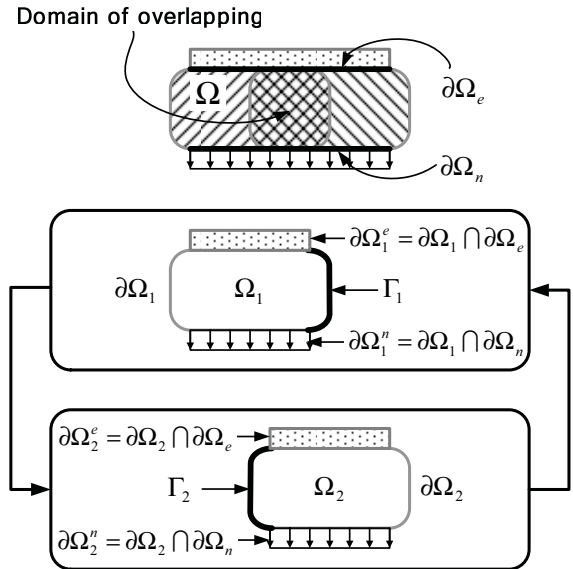


Figure 2: Analysis domain with two overlapping sub-domains.

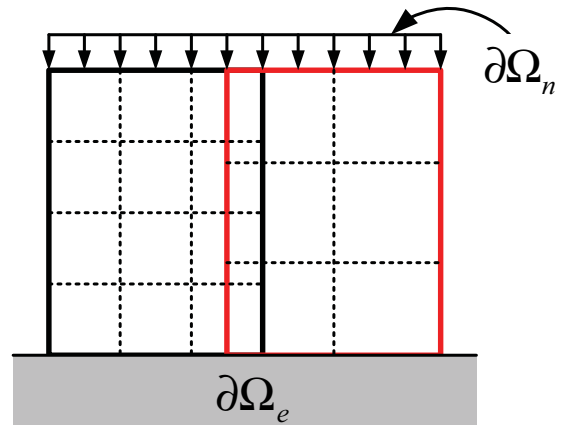


Figure 3: Finite element model composed of two overlapping finite element substructures.

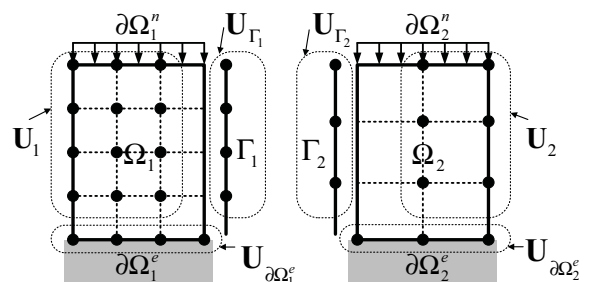


Figure 4: Decomposition of nodal variables of each sub-domain.

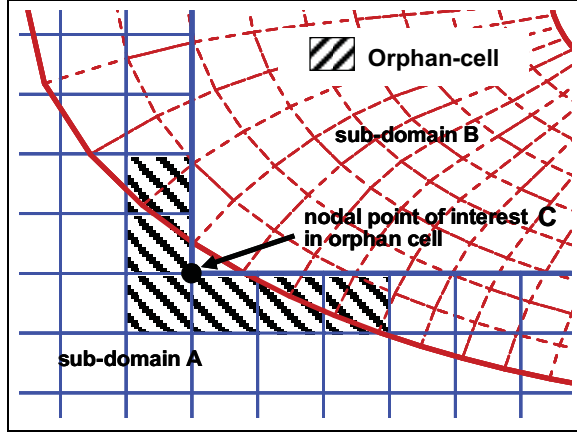


Figure 5: Overset grid with orphan-cell.

2.2 Moving Least Squares Approximation

In the present overset method, the MLS (moving least squares) approximation is employed to interpolate the required essential boundary values on the overlapped interface Γ_α ($1 \leq \alpha \leq 2$) from the result of the previous step obtained in the neighboring sub-domain.

The MLS method is one of the most popular meshless approximation schemes (along with RKPM [Liu, Jun and Chang (1995)], PUM [Babuska and Melenk (1997)], etc.) which do not need any well-defined mesh for data approximation. The required smoothness of approximation function can be easily achieved by the MLS method [Atluri (2005)].

Due to these reasons, the moving least squares technique may be a good candidate to approximate the required essential boundary values on the overlapped interface Γ_α ($1 \leq \alpha \leq 2$) from the result of the previous step obtained in the neighboring sub-domain with no regard to the existence of orphan-cell.

Consider the overlapped interface Γ_α for the sub-domain Ω_α , and suppose that the nodal values at the points \mathbf{x}_I ($1 \leq I \leq N$) in the neighboring sub-domain Ω_β ($\beta \neq \alpha$) are given as u^I . Then, to approximate the values of variable along the overlapped interface Γ_α for the sub-domain Ω_α , the approximate form (16) is defined as follows [Lancaster and Salkauskas (1981)].

For all $\mathbf{x} \in \Gamma_\alpha$,

$$u^h(\mathbf{x}) = \mathbf{p}^T(\mathbf{x})\mathbf{a}(\mathbf{x}) = \sum_{i=1}^m p_i(\mathbf{x})a_i(\mathbf{x}) \quad (16)$$

where $\mathbf{p}(\mathbf{x})$ is a complete monomial basis of order m , and $\mathbf{a}(\mathbf{x})$ is a vector containing coefficients $a_i(\mathbf{x})$ ($1 \leq i \leq m$). The basis $\mathbf{p}(\mathbf{x})$ is selected to contain constant '1', and to be linearly independent over some set of m among the given N points in Ω_β . The coefficients vector $\mathbf{a}(\mathbf{x})$ is determined by minimizing a weighted discrete L_2 error norm as follows.

$$\begin{aligned} \mathbf{a}(\mathbf{x}) &= \underset{\mathbf{b} \in \mathbb{R}^m}{\text{ARG}} [J(\mathbf{b})] \\ &= \underset{\mathbf{b} \in \mathbb{R}^m}{\text{ARG}} \left\{ [\mathbf{P}\mathbf{b} - \mathbf{V}_\beta]^T \mathbf{W}(\mathbf{x}) [\mathbf{P}\mathbf{b} - \mathbf{V}_\beta] \right\} \\ &= [\mathbf{P}^T \mathbf{W}(\mathbf{x}) \mathbf{P}]^{-1} [\mathbf{P}^T \mathbf{W}(\mathbf{x})] \mathbf{V}_\beta \end{aligned} \quad (17a)$$

where

$$\mathbf{P} = \begin{bmatrix} \mathbf{p}^T(\mathbf{x}_1) \\ \mathbf{p}^T(\mathbf{x}_2) \\ \vdots \\ \mathbf{p}^T(\mathbf{x}_N) \end{bmatrix} = \begin{bmatrix} p_1(\mathbf{x}_1) & \cdots & p_m(\mathbf{x}_1) \\ p_1(\mathbf{x}_2) & \cdots & p_m(\mathbf{x}_2) \\ \vdots & & \vdots \\ p_1(\mathbf{x}_N) & \cdots & p_m(\mathbf{x}_N) \end{bmatrix} \quad (17b)$$

$$\mathbf{V}_\beta = \begin{Bmatrix} u^1 \\ u^2 \\ \vdots \\ u^N \end{Bmatrix} \quad (17c)$$

$$\mathbf{W}(\mathbf{x}) = \begin{bmatrix} W_1(\mathbf{x}) & 0 & \cdots & 0 \\ 0 & W_2(\mathbf{x}) & \cdots & \vdots \\ \vdots & \vdots & \ddots & 0 \\ 0 & \cdots & 0 & W_N(\mathbf{x}) \end{bmatrix} \quad (17d)$$

The $N \times m$ matrix \mathbf{P} consists of basis, and the vector \mathbf{V}_β denotes the vector of given values u^I at nodes I ($1 \leq I \leq N$) in the sub-domain Ω_β . The $N \times N$ diagonal matrix $\mathbf{W}(\mathbf{x})$ is composed of weight functions. The weight function $W_I(\mathbf{x})$ is associated with the position \mathbf{x}_I of node I . The weight function $W_I(\mathbf{x})$ is selected to be non-negative for all \mathbf{x} , and the region of non-zero values is called the support. In computations, various kinds of weight functions can be adopted for MLS

approximation procedure. The required condition for the continuity of the approximation function can be easily satisfied by changing the weight function in the MLS approximation. In this work, the cubic spline weight function with a circular support is used.

$$W_I(\mathbf{x}) = \begin{cases} \frac{2}{3} - 4 \left(\frac{d_I}{R_I} \right)^2 + 4 \left(\frac{d_I}{R_I} \right)^3 & \text{for } 0 \leq \frac{d_I}{R_I} \leq \frac{1}{2} \\ \frac{4}{3} - 4 \left(\frac{d_I}{R_I} \right) + 4 \left(\frac{d_I}{R_I} \right)^2 - \frac{4}{3} \left(\frac{d_I}{R_I} \right)^3 & \text{for } \frac{1}{2} \leq \frac{d_I}{R_I} \leq 1 \\ 0 & \text{for } \frac{d_I}{R_I} \geq 1 \end{cases} \quad (18)$$

where R_I denotes the radius of support of weight function (range of influence) and d_I denotes the distance between the point of interest \mathbf{x} in Γ_α and nodal point \mathbf{x}_I in Ω_β .

Substituting $\mathbf{a}(\mathbf{x})$ obtained by Eq. (17) into Eq. (16) yields a relation which may be written in the form of a linear combination of nodal shape functions similar to that used in finite element method.

$$u^h(\mathbf{x}) = \Phi^T(\mathbf{x}) \mathbf{V}_\beta = \sum_{I=1}^N u^I \phi_I(\mathbf{x}) \quad (19)$$

where,

$$\begin{aligned} \Phi^T(\mathbf{x}) &= \mathbf{p}^T(\mathbf{x}) [\mathbf{P}^T \mathbf{W}(\mathbf{x}) \mathbf{P}]^{-1} \mathbf{P}^T \mathbf{W}(\mathbf{x}) \\ \phi_I(\mathbf{x}) &= \sum_{k=1}^m p_k(\mathbf{x}) [[\mathbf{P}^T \mathbf{W}(\mathbf{x}) \mathbf{P}]^{-1} \mathbf{P}^T \mathbf{W}(\mathbf{x})]_{kI} \end{aligned} \quad (20)$$

Additionally, Eq. (19) may be rewritten as Eq. (21) in terms of the decomposed nodal variables \mathbf{U}_β , $\mathbf{U}_{\Gamma_\beta}$, and $\mathbf{U}_{\partial\Omega_\beta^e}$ for the neighboring subdomain Ω_β defined in Fig. 4.

For $\mathbf{x} \in \Gamma_\alpha$,

$$u^h(\mathbf{x}) = \Phi_\beta^T(\mathbf{x}) \mathbf{U}_\beta + \Phi_{\Gamma_\beta}^T(\mathbf{x}) \mathbf{U}_{\Gamma_\beta} + \Phi_{\partial\Omega_\beta^e}^T(\mathbf{x}) \mathbf{U}_{\partial\Omega_\beta^e} \quad (21)$$

2.3 Connectivity Matrix Solution Procedure

Since the overset methods are based on the iterative Schwarz alternating scheme, an iterative solving technique has been conventionally used in the

overset methods. In the case of iterative solving scheme, the converged solution may be changed according to the convergence criteria and its tolerance [Varga (2000)]. Furthermore, it is not competitive to the direct solution scheme for the problems encountered in practical situations. Therefore, to reduce the solution time for the practical-sized problems, a new direct solution procedure is developed for a part of new overset method by using the concept of so-called ‘connectivity matrix’. As mentioned in the section 2.1, applying the Schwarz alternating procedure to the overlapping finite element system yields the set of equations, which are the same as Eqs. (10)-(13). And as the iteration number k goes to infinity, the solution for the iterative Eqs. (10)-(13) converges, and the converged solution satisfies the following equations in the limit.

$$[\mathbf{K}_{11} \quad \mathbf{K}_{1\Gamma_1}] \begin{Bmatrix} \mathbf{U}_1 \\ \mathbf{U}_{\Gamma_1} \end{Bmatrix} = \mathbf{F}_1 \quad (22)$$

$$[\mathbf{K}_{22} \quad \mathbf{K}_{2\Gamma_2}] \begin{Bmatrix} \mathbf{U}_2 \\ \mathbf{U}_{\Gamma_2} \end{Bmatrix} = \mathbf{F}_2 \quad (23)$$

$$\mathbf{U}_{\Gamma_1} = \Lambda(\mathbf{U}_2, \mathbf{U}_{\Gamma_2}, \bar{\mathbf{U}}_{\partial\Omega_2^e}) \quad (24)$$

$$\mathbf{U}_{\Gamma_2} = \Lambda(\mathbf{U}_1, \mathbf{U}_{\Gamma_1}, \bar{\mathbf{U}}_{\partial\Omega_1^e}) \quad (25)$$

Eq. (24) and Eq. (25), which are related to the interpolation of the nodal values in the overlapped interfaces, can be represented explicitly as shown below.

$$\mathbf{U}_{\Gamma_1} = \mathbf{C}_2^{(1)} \mathbf{U}_2 + \mathbf{C}_{\Gamma_2}^{(1)} \mathbf{U}_{\Gamma_2} + \mathbf{C}_{\partial\Omega_2^e}^{(1)} \bar{\mathbf{U}}_{\partial\Omega_2^e} \quad (26)$$

$$\mathbf{U}_{\Gamma_2} = \mathbf{C}_1^{(2)} \mathbf{U}_1 + \mathbf{C}_{\Gamma_1}^{(2)} \mathbf{U}_{\Gamma_1} + \mathbf{C}_{\partial\Omega_1^e}^{(2)} \bar{\mathbf{U}}_{\partial\Omega_1^e} \quad (27)$$

Further, Eqs. (26) and (27) can be rewritten by the so-called ‘connectivity matrix’ between the subdomains as shown in Eq. (28).

$$\underbrace{\begin{bmatrix} \mathbf{0} & -\mathbf{C}_2^{(1)} & \mathbf{I} & -\mathbf{C}_{\Gamma_2}^{(1)} \\ -\mathbf{C}_1^{(2)} & \mathbf{0} & -\mathbf{C}_{\Gamma_1}^{(2)} & \mathbf{I} \end{bmatrix}}_{\text{Connectivity Matrix}} \begin{Bmatrix} \mathbf{U}_1 \\ \mathbf{U}_2 \\ \mathbf{U}_{\Gamma_1} \\ \mathbf{U}_{\Gamma_2} \end{Bmatrix} = \begin{Bmatrix} \mathbf{C}_{\partial\Omega_2^e}^{(1)} \bar{\mathbf{U}}_{\partial\Omega_2^e} \\ \mathbf{C}_{\partial\Omega_1^e}^{(2)} \bar{\mathbf{U}}_{\partial\Omega_1^e} \end{Bmatrix} \quad (28)$$

The connectivity matrix plays a role of constraint which connects the overlapping sub-domains.

In case of the MLS approximation, the nodal points in the neighboring sub-domain, which influence the point of interest in the overlapped interface, are detected, and then the nodal shape functions are calculated. After that, the explicit form of connectivity matrix is constructed by using Eq. (21). It is noted that the number of nodal points, which influence the point of interest to be interpolated, should be no less than the order of monomial basis ‘ m ’ in order to prevent the singularity in the MLS approximation. Therefore, an automated selection procedure for the size of support (range of influence) is recommended in practical situations. This procedure is sketched in Fig. 6.

Finally, combining Eqs. (22), (23) and (28) yields Eq. (29).

$$\begin{bmatrix} \mathbf{K}_{11} & \mathbf{0} & \mathbf{K}_{1\Gamma_1} & \mathbf{0} \\ \mathbf{0} & \mathbf{K}_{22} & \mathbf{0} & \mathbf{K}_{2\Gamma_2} \\ \mathbf{0} & -\mathbf{C}_2^{(1)} & \mathbf{I} & -\mathbf{C}_{\Gamma_2}^{(1)} \\ -\mathbf{C}_1^{(2)} & \mathbf{0} & -\mathbf{C}_{\Gamma_1}^{(2)} & \mathbf{I} \end{bmatrix} \begin{Bmatrix} \mathbf{U}_1 \\ \mathbf{U}_2 \\ \mathbf{U}_{\Gamma_1} \\ \mathbf{U}_{\Gamma_2} \end{Bmatrix} = \begin{Bmatrix} \mathbf{F}_1 \\ \mathbf{F}_2 \\ \mathbf{C}_{\partial\Omega_2}^{(1)} \bar{\mathbf{U}}_{\partial\Omega_2^e} \\ \mathbf{C}_{\partial\Omega_1}^{(2)} \bar{\mathbf{U}}_{\partial\Omega_1^e} \end{Bmatrix} \quad (29)$$

It is noted that solving Eq. (29) gives the converged solution for the Schwarz alternating procedure with no iteration. Also, the solution is not dependent on the convergence criteria.

In this work, a special direct solver is developed, since the system matrix has a special form, which looks like an arrow, as shown in Fig. 7. To increase the computing efficiency, the system matrix is stored separately into three parts (e.g., diagonal part, right part, and bottom part), and the operations for the other parts are excluded.

To investigate the efficiency of the proposed connectivity matrix solution procedure, the solution time is compared with that required in the conventional SOR-type iterative scheme. For the problem with 280 degrees of freedom, the proposed connectivity matrix solution procedure required

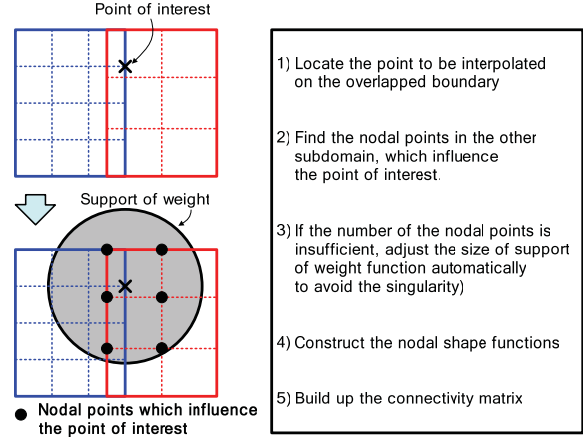


Figure 6: Constructing the connectivity matrix through the MLS approximation.

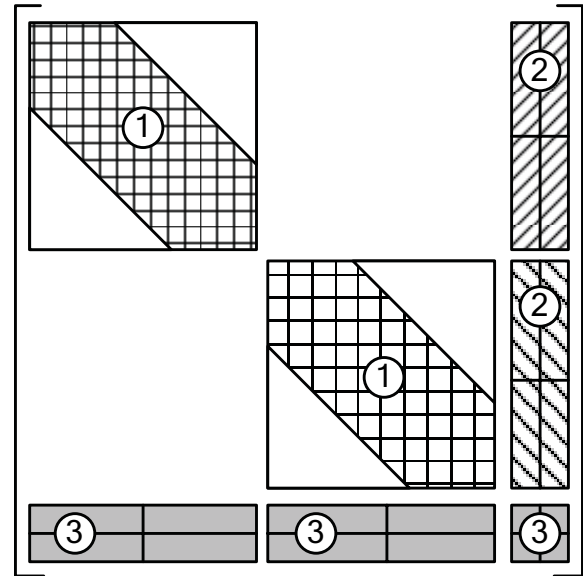


Figure 7: Separate Storage for the system matrix of the integrated whole model.

only 0.34 sec, whereas it took 55.8 sec in the SOR-type iterative scheme with the error tolerance 10^{-7} . In Fig. 8, the solution times are presented up to the problem with six thousand degrees of freedom. The results show that the proposed connectivity matrix solution procedure is much more efficient than the conventional iterative solution procedure as the number of total degrees of freedom is increased.

From the results, it is identified that one can greatly reduce the computational time, required

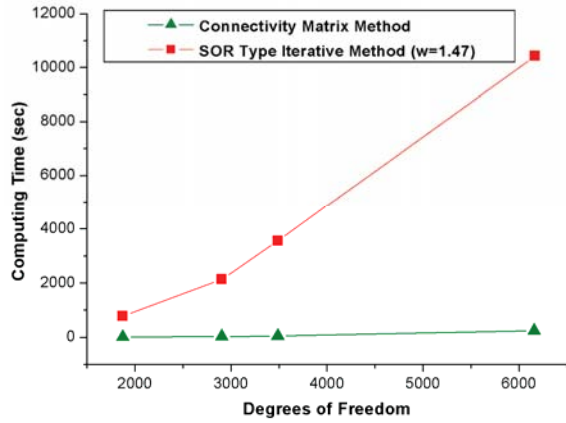


Figure 8: Comparison of computational time of the connectivity matrix solution procedure with that of the iterative solution procedure.

in the coupled analysis of independently modeled overlapping finite element substructures, through the connectivity matrix solution procedure.

3 Numerical examples

To investigate the performance and the potential of the proposed overset method, several numerical examples are worked out. In all of the numerical examples, the bilinear quadrilateral element is utilized, and the second order monomial basis is used for the MLS approximation.

3.1 Patch Test

The patch tests are carried out to prove the validity of the currently proposed overset method in this section. For the patch tests, two models in Fig. 9 are considered. The first model consists of two overlapping finite element substructures of which nodal points are compatible with each other. The second model has nodal incompatibility in the overlapping region of two finite element substructures.

Young’s modulus and Poisson’s ratio are $E=1$ and $\nu=0.3$, respectively, and the support size is selected as 2.1 times the nodal distance. As presented in table 1, one can identify that the proposed overset method gives a quite acceptable solution in a practical sense.

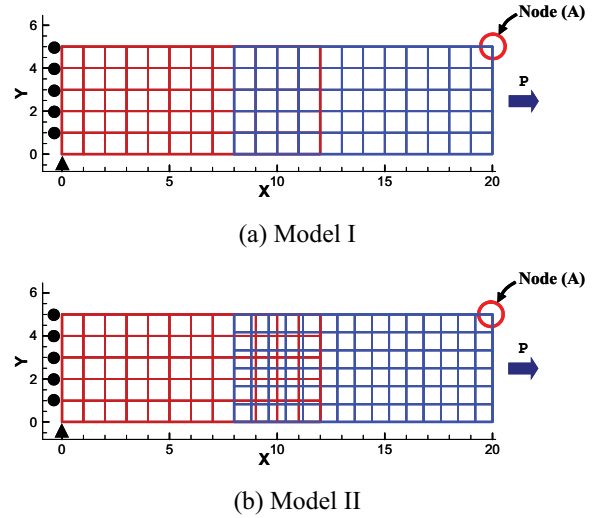


Figure 9: Models for the patch tests.

Table 1: Displacements of node A from the patch tests.

Node A	u	v
Exact	20	-1.5
Model I	19.9999999	-1.5
Model II	20.0000324	-1.50005183

3.2 Beam Type Problem

To investigate the convergence character of the proposed overset method, a cantilevered beam type problem is analyzed. The beam of length $L=20$ with thickness $h=2$ in Fig. 10 is assumed in the plane stress state. Young’s modulus and Poisson’s ratio are $E = 1 \times 10^7$ and $\nu=0.3$, respectively. The shear force $P=2000$ is applied to the right-hand side of the beam, and the fixed essential boundary condition is enforced on the left-hand side of the beam. The substructures are discretized by the different size of mesh, and 2.1 times the nodal distance is chosen as the support size of the weight function. The exact displacements are given as follows.

$$u = \frac{P}{6EI} \times \left(y - \frac{h}{2} \right) [3x(x - 2l) + (\nu + 2)(h - y)y] \quad (30a)$$

$$v = \frac{P}{6EI} \left[x^2(3l-x) - 3v(x-l) \left(y - \frac{h}{2} \right)^2 + (4+5v) \frac{h^2}{4} x \right] \quad (30b)$$

where I denotes the area moment of inertia of the beam cross-section. The corresponding stresses are as follows.

$$\sigma_{xx} = \frac{P}{I}(x-L) \left(y - \frac{h}{2} \right) \quad (31a)$$

$$\sigma_{yy} = 0 \quad (31b)$$

$$\sigma_{xy} = \frac{Py}{2I} \left(\frac{h}{2} - y \right) \quad (31c)$$

For the convergence test, meshes in each subdomain are refined, and the results are presented in Fig. 11 and table 2. The convergence rate for the L_2 error norm is 2. From the results, it is observed that the convergence rate according to the mesh refinement is similar to that of the conventional finite element method. In Fig. 12, the deformed shape obtained by the coupled analysis of whole model is presented.

Table 2: Error norms for each mesh division.

Case	Mesh Size		L_2 Norm
	Ω_1	Ω_2	
1	0.5	0.4	6.35×10^{-4}
2	0.25	0.2	1.63×10^{-4}
3	0.125	0.1	4.12×10^{-5}
4	0.0625	0.05	1.03×10^{-5}
5	0.03125	0.025	2.57×10^{-6}

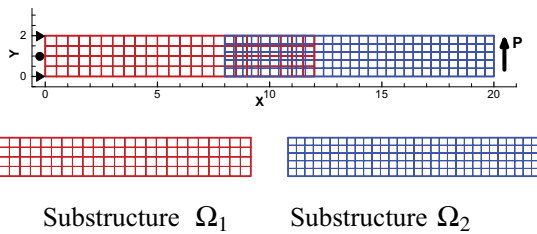


Figure 10: Beam type overlapping model with nodal incompatibility.

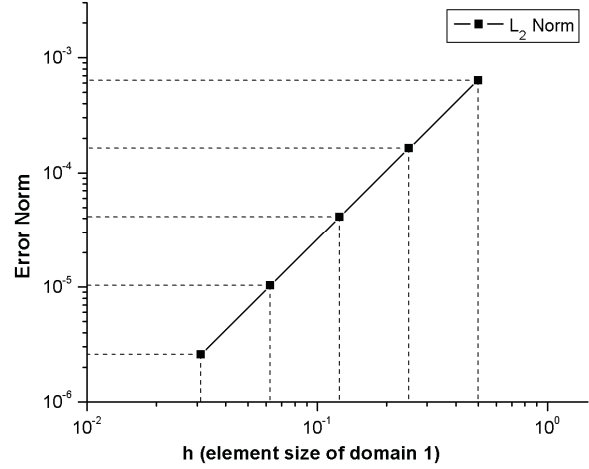


Figure 11: Convergence rate for L_2 error norm.

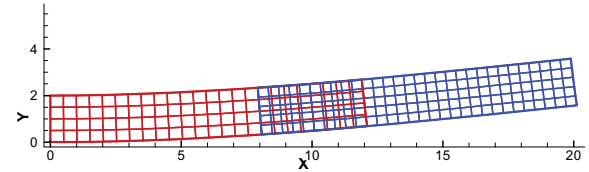


Figure 12: Deformed shape obtained by the coupled analysis of whole model.

3.3 Infinite Plate with Circular Hole

The second model for the convergence test is an infinite plate with a circular hole under the uniform traction $p = 100$. By using the symmetry of the model, only a quarter of the model is considered in the analysis as shown in Fig. 13. The essential boundary condition is enforced on both of the left-hand side and the bottom side. As a natural boundary condition, the exact traction obtained from the exact solution is applied to the right-hand side and the upper side of the model. For Young's modulus and Poisson's ratio, $E = 3 \times 10^3$ and $\nu = 0.3$ are used, respectively. For this problem, the exact solutions are given as follows.

$$u = \frac{1+\nu}{E} p \left(\frac{1}{1+\nu} r \cos \theta + \frac{2}{1+\nu} \frac{a^2}{r} \cos \theta + \frac{1}{2} \frac{a^2}{r} \cos 3\theta - \frac{1}{2} \frac{a^4}{r^3} \cos 3\theta \right) \quad (32a)$$

$$v = \frac{1+\nu}{E} p \left(\frac{-\nu}{1+\nu} r \sin \theta - \frac{1-\nu}{1+\nu} \frac{a^2}{r} \sin \theta + \frac{1}{2} \frac{a^2}{r} \sin 3\theta - \frac{1}{2} \frac{a^4}{r^3} \sin 3\theta \right) \quad (32b)$$

$$\sigma_{xx} = p \left(1 - \frac{a^2}{r^2} \left(\frac{3}{2} \cos 2\theta + \cos 4\theta \right) + \frac{3a^4}{2r^4} \cos 4\theta \right) \quad (32c)$$

$$\sigma_{xy} = p \left(-\frac{a^2}{r^2} \left(\frac{1}{2} \sin 2\theta + \sin 4\theta \right) + \frac{3a^4}{2r^4} \sin 4\theta \right) \quad (32d)$$

$$\sigma_{yy} = p \left(-\frac{a^2}{r^2} \left(\frac{1}{2} \cos 2\theta - \cos 4\theta \right) - \frac{3a^4}{2r^4} \cos 4\theta \right) \quad (32e)$$

The L_2 error norms are presented in table 3, and the convergence rate is plotted in Fig. 14. In table 3, mesh division ($n_r \times n_\theta$) for the sub-domain Ω_1 denotes that the sub-domain Ω_1 is divided by n_r -elements in the radial direction and n_θ -elements in the circumferential direction, respectively. For the sub-domain Ω_2 , the size of element is denoted. Similar to the case of the beam type problem, the convergence rate for the L_2 error norm is 2 as shown in Fig. 14.

In Fig. 15, the maximum value of σ_{xx} near the hole is presented according to the mesh refinement. One can observe that the maximum stress value approaches the exact stress value ($\sigma_{max}=300$). From the numerical results, it is validated that the proposed overset method has a reasonable convergence rate.

Table 3: Error norms for each mesh refinement.

Case	Mesh division	Mesh size	L_2 norm
	Ω_1	Ω_2	
1	3×4	1	1.32×10^{-3}
2	6×8	0.5	3.70×10^{-4}
3	12×16	0.25	1.00×10^{-4}
4	24×32	0.125	2.58×10^{-5}
5	48×64	0.0625	6.40×10^{-6}
6	96×128	0.0315	1.54×10^{-6}

3.4 Practical Tunnel model

A practical tunnel model is analyzed by using the proposed overset method in this section. The tunnel model is modeled by two overlapping finite element substructures as shown in Fig. 16, where the inside substructure has a finer mesh system when compared with the outside substructures. Using the symmetry of the model, the essential boundary condition is enforced on both of the left-hand side and the bottom side of the model, and

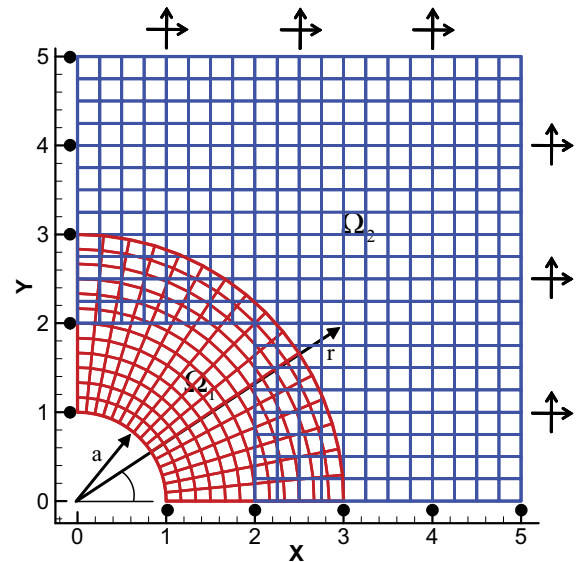


Figure 13: A quarter of the plate with a circular hole made of two overlapping finite element substructures.

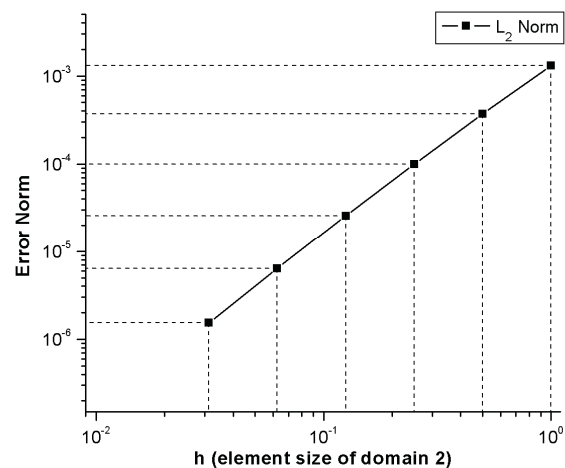


Figure 14: Convergence rate for L_2 error norm.

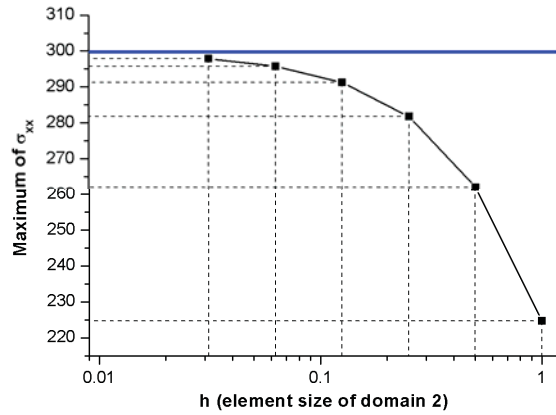


Figure 15: Maximum value of σ_{xx} near the hole.

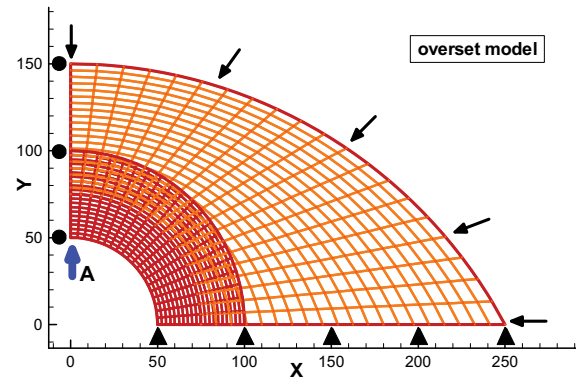


Figure 16: Tunnel model composed of two finite element substructures.

Table 4: The number of nodes and the number of elements for each model.

Case	No. of nodes		No. of elements	
FEM I	336		300	
FEM II	1271		1200	
FEM III	4941		4800	
Overset Model	Ω_1	Ω_2	Ω_1	Ω_2
	651	441	600	400

Table 5: Comparison of deflections at point A.

	FEM I	FEM II	FEM III	Overset Method
Point A	-17.4423	-17.5252	-17.5462	-17.5492

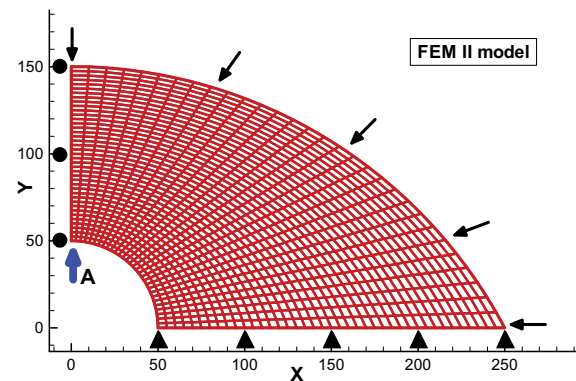


Figure 17: Finite element model with compatible mesh geometry.

the distributed load $p=1000$ is applied to the upper side of the model. Young's modulus and Poisson's ratio are $E = 1 \times 10^4$ and $\nu = 0.3$, respectively.

In order to assess the performance of the proposed overset method, the finite element analyses are also carried out for the models with compatible mesh geometry as shown in Fig. 17. In table 4, the number of nodes and the number of elements for each model are presented. The deflections of point A obtained by each method are compared with each other in table 5. The comparison shows that the current overset method gives a reliable solution. Moreover, it is known that the proposed overset method makes it possible to improve the numerical solution by simply substituting the fine mesh substructure for the region of stress concentration without considering the overlapping between the finite element substructures.

3.5 Model with Orphan-Cell

In real practice, the orphan-cell is often produced unintentionally during the modeling procedures. Therefore, it is essential to eliminate the problem of orphan-cell for more practical applications of overset method, since the previous overset methods, which rely on the mesh-dependent interpolation techniques, have been plagued by the problem of orphan-cell.

Due to this reason, the applicability of the proposed overset method, which uses the mesh-independent MLS approximation, is investigated for the three models with orphan-cells presented in Fig. 18. The first model is an infinite plate with a circular hole, and in the model there is an orphan-cell near the overlapping region as shown in Fig. 18a. The second model is a beam type

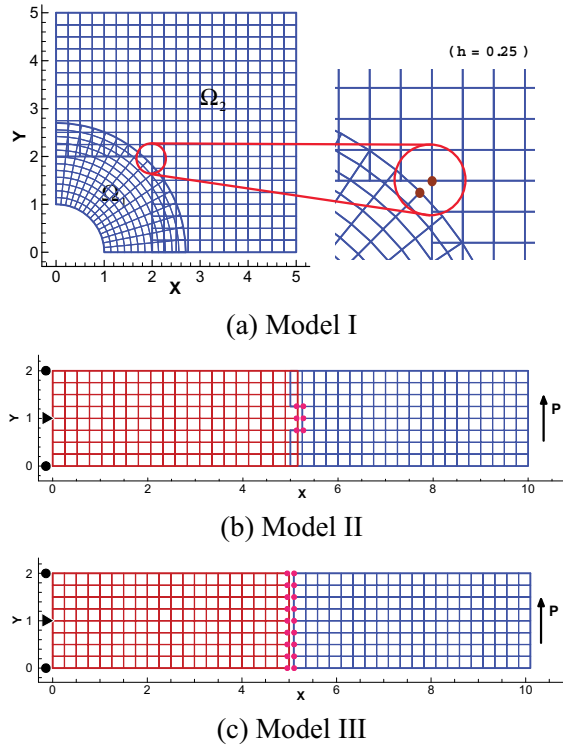


Figure 18: Various models with orphan-cell composed of two finite element substructures.

model composed of two overlapping substructures with orphan-cells as presented in Fig. 18b. In the final model in Fig. 18c, two finite element substructures are located at a distance with no overlapping.

In Fig. 19, the analysis results for each model are presented according to the support size of the MLS weight function (i.e., the size of domain of influence). In the results, it is observed that the magnitudes of errors in the numerical solutions, obtained by the proposed overset method, are relatively small (less than 0.5% for all cases), whereas it is highly difficult to obtain a reasonable solution for the model with orphan-cell by using the previously developed overset methods. Additionally, it is shown that the smallest support size, which does not induce the singularity, gives an acceptable result for the model with orphan-cell.

From the results, it is confirmed that the coupled analysis of the overlapping model with orphan-cell can be carried out with no difficulty through the proposed overset method.

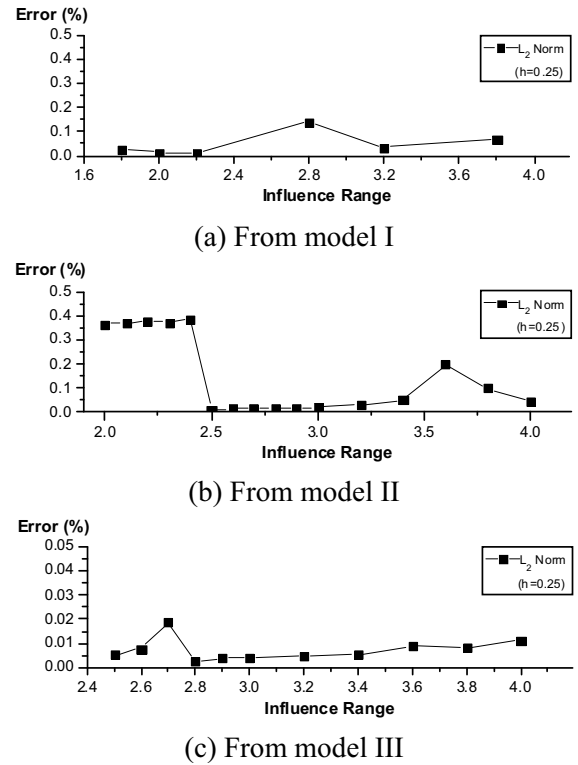


Figure 19: Relative error norm according to the support size of weight function (the range of influence).

4 Conclusions

In this work, a novel overset method is proposed for coupled analysis of independently modeled overlapping finite element substructures. To interpolate the boundary data for the overlapped interface from the neighboring sub-domain, the MLS (moving least squares) approximation is used instead of the Lagrange interpolation method, which has been conventionally used in the previous overset methods. And as a result, a problem of interpolation, induced by the existence of orphan-cell in the traditional overset methods, is greatly alleviated.

Further, the connectivity matrix is derived from the limit conditions for the converged solution of the Schwarz alternating procedure. And by using the connectivity matrix, a novel direct solving procedure is developed. Through the connectivity matrix solution procedure, the computing time is greatly reduced when compared with the conven-

tional iterative solving procedure. Additionally, the converged solution can be obtained with no iteration, and the need for convergence criteria is completely eliminated.

To investigate the validity and performance of the proposed method, various numerical examples are worked out, including the patch tests, the convergence tests, and the models with orphan-cell. From the numerical examples, it is confirmed that the proposed overset method passes the patch test in a practical sense, and gives a reasonable convergence rate. Moreover, the flexibility in dealing with the overlapping model with orphan-cell is demonstrated. Additionally, it is known that the proposed method is also useful in improving the numerical solution by substituting the fine mesh substructures for the region of stress concentration with no regard to the overlapping of substructures. From the results, it is identified that the proposed orphan-cell-free overset method is efficient in performing the coupled analysis of independently modeled overlapping finite element substructures. Further, it is confirmed that it has a great potential in practical situations such as collaborative engineering procedures.

Acknowledgement: This work was supported by Korea Research Foundation Grant (KRF-2006-311-D00039). Authors would like to acknowledge the financial support from the Korea Research Foundation.

References

- Aminpour, M.A; Pageau, S.; Shin, Y.** (2001): Improved interface modeling technology. *Proceeding of 42nd AIAA/ASME/ASCE/AHS/ASC Structures, Structural Dynamics, and Material Conference*, Paper No. AIAA-2001-1548.
- Aminpour, M.A; ransom, J.B; McCleary, S.L.** (1995): A coupled analysis method for structures with independently modeled finite element subdomains. *International Journal for Numerical Methods in Engineering*, Vol. 38, pp. 3695-3718.
- Atluri, S.N.** (2005): *Methods of Computer Modeling in Engineering & the Sciences*, Vol. 1. Tech Science Press, Forsyth, GA.
- Atluri, S.N.; Cho, J.Y.; Kim, H.S.** (1999): Analysis of thin beams, using the meshless local Petrov-Galerkin method, with generalized moving least squares interpolations. *Computational Mechanics*, Vol. 24, pp. 334-347.
- Babuska, I.; Melenk, J.** (1997): The partition of unity method. *International Journal for Numerical Methods in Engineering*, Vol. 40, pp. 727-758.
- Cho, J.Y.** (2007): How to achieve Kronecker delta condition in moving least squares approximation along the essential boundary. *CMC: Computers, Materials, & Continua*, Vol. 5, pp. 99-116.
- Cho, J.Y.; An, J.M.; Song, Y.M.; Lee, S.; Choi, D.W.** (2005): Coupled analysis of independently modeled finite element substructures by moving least squares displacement welding technique. *CMES: Computer Modeling in Engineering & Sciences*, Vol. 9, pp. 1-17.
- Cho, K.W.; Kwon, J.H.; Lee, S.** (1999): Development of a fully systemized chimera methodology for steady/unsteady problems. *Journal of Aircraft*, Vol. 36, pp. 973-980.
- Chung, S.W.; Choi, Y.J.; Kim, S.J.** (2003): Computational simulation of localized damage by finite element remeshing based on bubble packing method. *CMES: Computer Modeling in Engineering & Sciences*, Vol. 4, pp. 707-718.
- Han, Z.D.; Atluri, S.N.** (2002): SGBEM (for cracked local subdomain) – FEM (for uncracked global structure) alternating method for analyzing 3D surface cracks and their fatigue growth. *CMES: Computer Modeling in Engineering & Sciences*, Vol. 3, pp. 699-716.
- Lancaster, P.; Salkauskas, K.** (1981): Surfaces generated by moving least squares methods. *Mathematics of Computation*, Vol. 37, pp. 141-158.
- Lee, S.; Park, M.; Cho, K.W.; Kwon, J.H.** (2000): New fully automated procedure for the prediction of store trajectory. *Journal of Aircraft*, Vol. 37, pp. 1038-1049.
- Li, X.Y.; Teng, S.H.; Wan, P.J.** (2001): To generate good triangular meshes, conforming to control spacing requirements. *CMES: Computer Model-*

ing in *Engineering & Sciences*, vol. 2, pp. 97-115.

Lions, P.L. (1987): On the Schwarz alternating method I. *SIAM Proceeding of the First International Symposium on Domain Decomposition Methods for Partial Differential Equations*, pp. 1-42.

Liu, J.; Sun, S.; Wang, D. (2006): Optimal tetrahedralization for small polyhedron: a new local transformation strategy for 3-D mesh generation and mesh improvement. *CMES: Computer Modeling in Engineering & Sciences*, Vol. 14, pp. 31-43.

Liu, W.; Jun, S.; Zhang, Y. (1995): Reproducing kernel particle methods. *International Journal for Numerical methods in Fluid*, Vol. 20, pp. 1081-1106.

Nie, Y.F.; Atluri, S.N.; Zuo, C.W. (2006): The optimal radius of the support of radial weights used in moving least squares approximation. *CMES: Computer Modeling in Engineering & Sciences*, Vol. 12, pp. 137-148.

Park, K.C; Felippa, C.A. (2000): A variational principle for the formulation of partitioned structural systems. *International Journal for Numerical Methods in Engineering*, Vol. 47, pp. 395-418.

Schwarz, H.A. (1869): Über einige abbildungsaufgaben. *Ges. Math. Abh.*, Vol. 11, pp.65-83.

Steger, J.L.; Benek, J.A. (1987): On the use of composite grid schemes in computational aerodynamics. *Computer Methods in Applied Mechanics and Engineering*, Vol. 64, pp. 301-320.

Varga, R.S. (2000): *Matrix Iterative Analysis*. 2nd Revised and Expanded Ed., Springer-Verlag, Berlin.

Vodička, R.; Mantič, V.; París, F. (2007): Symmetric variational formulation of BIE for domain decomposition problems in elasticity – an SGBEM approach for nonconforming discretizations of curved interfaces. *CMES: Computer Modeling in Engineering & Sciences*, Vol. 17, pp. 173-203.

Wang, L.; Atluri, S.N. (1996): Recent Advances

in the Alternating Method for Elastic and Inelastic Fracture Analyses. *Computer Methods in Applied Mechanics and Engineering*, Vol. 137, pp. 1-58.

Wijesinghe, H.S.; Hadjiconstantinou, N.G. (2004): A hybrid atomistic-continuum formulation for unsteady, viscous, incompressible flows. *CMES: Computer Modeling in Engineering & Sciences*, Vol. 5, pp. 515-526.